Mechanical Response of Shallow Crust to Groundwater Storage Variations: Inferences from Deformation and Seismic Observations in the Eastern Southern Alps, Italy

F. Pintori[1,2], E. Serpelloni[1], L. Longuevergne[3], A. Garcia-Aristizabal[1], M. E. Belardinelli[2], L. Faenza[1], L. D'Alberto[4], A. Gualandi[5,6]

[1]Istituto Nazionale di Geofisica e Vulcanologia, Italy.

[2]Università di Bologna, Dipartimento di Fisica e Astronomia, Settore di Geofisica, Bologna, Italy.

[3]ARPA Veneto, Inland Waters Office, Padova, Italy.

[4]Geosciences Rennes, UMR CNRS 6118, Université de Rennes 1,Rennes, France.

[5]Department of Geological and Planetary Sciences, California Institute of Technology, Pasadena, CA, USA.

[6]Jet Propulsion Laboratory, California Institute of Technology, Pasadena, CA, USA.

Corresponding author: Francesco Pintori (francesco.pintori@ingv.it)

Key Points:

- Changes in terrestrial water storage modulate horizontal transient deformation
- Pressure changes in shallow fractures cause large stress changes at seismogenic depth
- Background seismicity rates are correlated with terrestrial water content

Abstract

It is known that changes in continental water storage can produce vertical surface deformation, induce crustal stress perturbations and modulate seismicity rates. However, the degree to which local changes in terrestrial water content influence crustal stresses and the occurrence of earthquakes remains an open problem. We show how changes in terrestrial water storage, computed for a ~1000 km^2 basin, focus deformation in a narrow zone, causing horizontal, non-seasonal displacements. We present results from a karstic mountain range located at the edge of the Adria-Eurasia plate boundary system in northern Italy, where shortening is accommodated across an active fold-and-thrust belt. The presence of geological structures with high permeabilities and of deeply rooted hydrologically-active fractures focus groundwater fluxes and pressure changes, generating transient horizontal deformation and perturbations of crustal stress up to 25 kPa, at seismogenic depths. The background seismicity rates appear correlated, without evident temporal delay, with the terrestrial water content in the hydrological basin. Being independent from hydraulic diffusivity, seismicity modulation is likely affected by direct stress changes on faults planes.

Plain Language Summary

Recognizing non-seasonal deformation associated with groundwater level changes is mandatory for improving the accuracies of tectonic deformation rates and for detecting small tectonic transient deformation. Here we present the results obtained from the analysis of ground GNSS displacements time-series integrated by hydrological and mechanical modeling in the Eastern Southern Alps. We find that water convergence toward a hydrologically-conductive zone can generate mm-scale horizontal surface displacements. Furthermore, we prove that water accumulation can generate stress changes large enough to influence the rates of the seismic events occurrence.

Keywords: GNSS; hydrology; non-tectonic deformation; stress changes; seismicity rates; Alps

1 Introduction

Constant redistribution of surface loads due to continental hydrology (van Dam et al., 2001) causes measurable deformation of the Earth's surface. In particular, seasonal hydrological mass movements turned out to influence tectonic deformation of the lithosphere and modulate seismicity rates in several tectonic environments (e.g., Bettinelli et al., 2008; Craig et al., 2017; Johnson et al., 2019; Lowry, 2006). While seasonal modulation of seismicity associated with vertical loading is a known process, hydrologically-driven deformation mainly acting on the horizontal components have been more recently recognized. Silverii et al. (2020) describe horizontal seasonal deformation caused by poroelastic processes related to snowmelt runoff water infiltrating into the Sierra Nevada slopes around Long Valley Caldera (USA); Oestreicher (2018) shows repetitive and reversible horizontal movements of up to ∼55mm on annual scales, strongly correlated with modeled groundwater levels in Southern Alps (New Zealand); Silverii et al. (2016) recognize transient deformation signals in GPS horizontal time series, controlled by seasonal and interannual phases of groundwater recharge/discharge of karst aquifers in the Apennines (Italy); Devoti et al (2015) and Serpelloni et al. (2018) describe horizontal transient deformation signals in the Southern Alps (Italy), correlated with precipitation.

Both in the Apennines and in the Alps, changes in groundwater levels in karst aquifers, or fractures associated with karst systems, are considered the most likely mechanisms to explain the observed deformation, which is characterized by larger displacements in the horizontal components than in the vertical one. Since direct measurements of groundwater levels at mesoscale are difficult to obtain, particularly in mountain regions, such as in the study area (see Fig. 8 from Chen et al., 2018), the hydrological nature of these aforementioned deformation signals has been suggested based on temporal correlation between geodetic displacements and meteorological and hydrological data like precipitation, spring discharge, river flow, snow water equivalent and lake levels. The Gravity Recovery and Climate Experiment (GRACE) provides complementary independent observations of total water mass (Equivalent Water Thickness, EWT), but its spatial resolution is lower than scales of 300 km (Famiglietti et al., 2011). As a result, at spatial scales significantly lower than the GRACE resolution, when direct measurements of groundwater contents are not available (e.g, because of the lack of water wells) the geodetic signals are more often correlated with groundwater proxy data (mainly precipitation and spring discharge). Serpelloni et al. (2018) studying the Adria-Eurasia plate boundary in Italy and Slovenia showed that detected geodetic transient signals are poorly correlated with daily precipitation data, but highly correlated, without temporal delay, with the history of cumulated precipitations at monthly time scales. However, the physical interpretation of this monthly-scale cumulative precipitation signal, in terms of hydrological cycle and groundwater changes, is not straightforward.

Identifying and extracting non-tectonic signals from geodetic measurements remains critical to detect potential tectonic signals of small amplitude and to improve the accuracy and precision of interseismic deformation estimates. Moreover, studying hydrological deformation signals can provide new clues on elastic (Chanard et al., 2014; Drouin et al., 2016) and viscoelastic (Chanard et al., 2018) properties of the Earth, on continental water storage fluctuations (Borsa et al., 2014; Fu et al., 2013) and on the possible relationship between hydrologically-driven stress changes and earthquake nucleation. Two mechanisms by which hydrology can modulate earthquake occurrence have been suggested: variations in pore-fluid pressure at hypocentral depths (Hainzl et al., 2006) and direct stress on the fault plane (Bettinelli et al., 2008; Craig et al., 2017; D'Agostino et al., 2018; Johnson et al., 2017). An effective way to discriminate between these two processes is the presence of a time lag between hydrological indicators and seismicity rates. In fact, while the effect of the direct stress can be considered instantaneous, hydraulic diffusivity at hypocentral depth determine a time lag between hydrological and seismological indicators, if pore-fluid pressure variations are the main driver of earthquake rates modulation.

In this work we study a segment of the Adria-Eurasia plate boundary in North-Eastern Italy (Fig. 1), hit by strong historical earthquakes (e.g, the Mw 6.5, 1695 Asolo earthquake; Rovida et al., 2020) and where the larger part of plate convergence is presently accommodated across a south-vering fold-and-thrust belt (Anderlini et al., 2020; Serpelloni et al., 2016). The main thrusts are, from the internal parts to the foreland, the Valsugana thrust, the Belluno thrust and the Bassano-Valdobbiadene thrust (BVT), the latter being associated with a morphological relief of ~1200 m above the plain, known as Pedemountain flexure (Fig. 1). The southernmost active front is now mainly buried beneath the alluvial deposits of the Venetian plain and sealed by Late Miocene to Quaternary (~7–2.5 Ma) deposits (Fantoni et al., 2002), consisting in the Montello thrust (Fantoni et al., 2002; Galadini et al., 2005). The Montello hill (Fig. 1) is generally interpreted as an actively growing ramp anticline on top of the north dipping thrust that has migrated south of the mountain into the foreland (Serpelloni et al., 2016).

The main geomorphological feature of the area is the presence of the NE-SW oriented Belluno Valley, where the Piave river flows, bounded to the north by the Dolomites and to the south by the Monte Grappa massif, the Monte Cesen-Col Visentin (MCCV) mountain chain and the Alpago-Cansiglio plateau (see Fig. 1). The MCCV is the morphological expression of an anticline associated with the BVT and back thrust system, and it is crossed by the Piave river that flows to the southeast reaching the Montello hill. Highly productive fissured, hydrologically independent, karst aquifers are present in the area (Fig. 3; Filippini et al., 2018): in the Dolomites, one associated with the MCCV and one with the Alpago-Cansiglio plateau.

In this work we link hydrology to crustal deformation and geological structures by adopting physically-based models constrained by precipitation, temperature and river flow data and subsurface geological information. We show how water collected in a ~1000 km^2 basin focuses groundwater fluxes and pressure changes in a relatively narrow geological structure, generating transient horizontal deformation and perturbations of crustal stress of up to 25 kPa at seismogenic depths. Finally, we study the correlation between total water storage (TWS) changes and seismicity rates through a statistical approach.

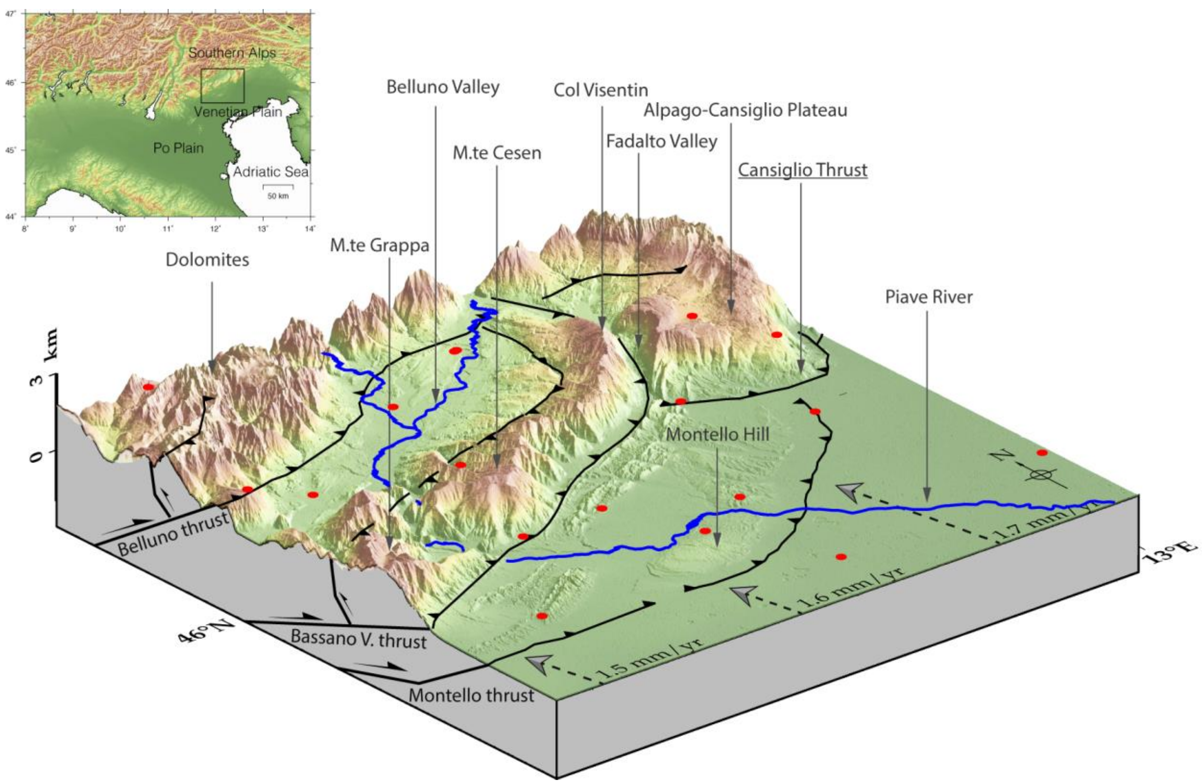

Figure 1. 3D view (from SW) of the study area. The dashed arrows indicate the Adria-Eurasia convergence rate and direction, predicted from a GNSS-derived rotation pole (Serpelloni et al., 2016). The digital elevation model, with topographic exaggeration, is obtained from ALOS Global Digital Surface Model data. The black lines represent the major fault lines (fault names are reported in the vertical section or with underlined text). The red dots indicate the position of the GPS stations.

2 GNSS data and time-series analysis

In this work we extended the analysis carried out by Serpelloni et al. (2018), including more stations and a longer time-span, focusing on one specific sector (Fig. 1). The displacement time-series from GNSS stations in the 2010.0-2019.3 time span (Fig. 2 and Supplementary Fig. S1), obtained following the procedures described in the Supplementary Text S1, have been analyzed with a blind source separation algorithm based on variational Bayesian Independent Component Analysis (vbICA; Gualandi et al., 2016). This method has been successfully used to extract hydrological and tectonic transient signals from GNSS displacements time series (Gualandi et al., 2017a; Gualandi et al., 2017b); it uses a generative model to recreate the observations and allows extracting the spatiotemporal information of independent sources of deformation directly from the observations, without imposing any specific spatial distribution or temporal function.

The output of this analysis is the definition of a limited number of sources, or components, characterized by a specific spatial distribution (U) and following a specific temporal evolution (V). A weight coefficient S (in mm) is necessary to rescale their contribution in explaining the original data. Each independent component (IC) is described by a mix of Gaussians, which allows for more flexibility in the description of the sources with respect to classical independent component analysis (ICA) techniques. It allows to consistently take into account missing data in the data set (Chan et al., 2003) and provides an estimate of the uncertainty associated with each IC. The displacement time series at a given station can be reconstructed by linearly summing up the contributions from all the ICs, each of which is obtained by multiplying the specific spatial distribution by the associated weight times the temporal evolution.

With the goal of reducing the correlation of the data set, the original time series are initially detrended, which results in a more efficient search of the IC direction (Gualandi et al., 2016). Differently from Serpelloni et al. (2018), the trend of each GPS station is estimated in a multivariate statistical manner, by applying a vbICA analysis on displacement-time series realized in a Adria-fixed reference frame, as described in the Supplementary Text S1.2. This approach is effective in removing the linear trend in case of strong non-linear signals and short time-series.

Once detrended, according to the F-test, 3 ICs are necessary to satisfactorily reconstruct the observed displacements. The temporal evolution (V) and spatial responses (U) of the three ICs are shown in Fig. 2. Seasonal annual displacements in the vertical and NS directions (IC1 and IC3) occur in response to surface hydrological mass loading (Serpelloni et al., 2018). A non-seasonal, horizontal transient deformation signal (IC2, Fig. 2), characterized by spatially variable amplitudes and directions, causes GNSS stations to reverse the sense of movement with time, resulting in a sequence of dilatational and compressional deformation oriented about normal to the mountain front.

Serpelloni et al. (2018) found that the temporal evolution of this signal somehow correlates with the history of cumulated precipitations at monthly timescales. Nonetheless, the link between surface deformation and changes in groundwater content remains difficult to find, because of the lack of water wells in the mountainous areas and because of the limited spatial extent of the area affected by this transient geodetic deformation signal. EWT values estimated from GRACE have a spatial resolution larger than 300 km (Famiglietti et al., 2011), with a monthly temporal resolution. In the next section we use a lumped parameter hydrological model to estimate daily changes of continental water content to be compared with the temporal evolution of IC2, studying the link between changes in groundwater level, geological structures and local seismicity rates.

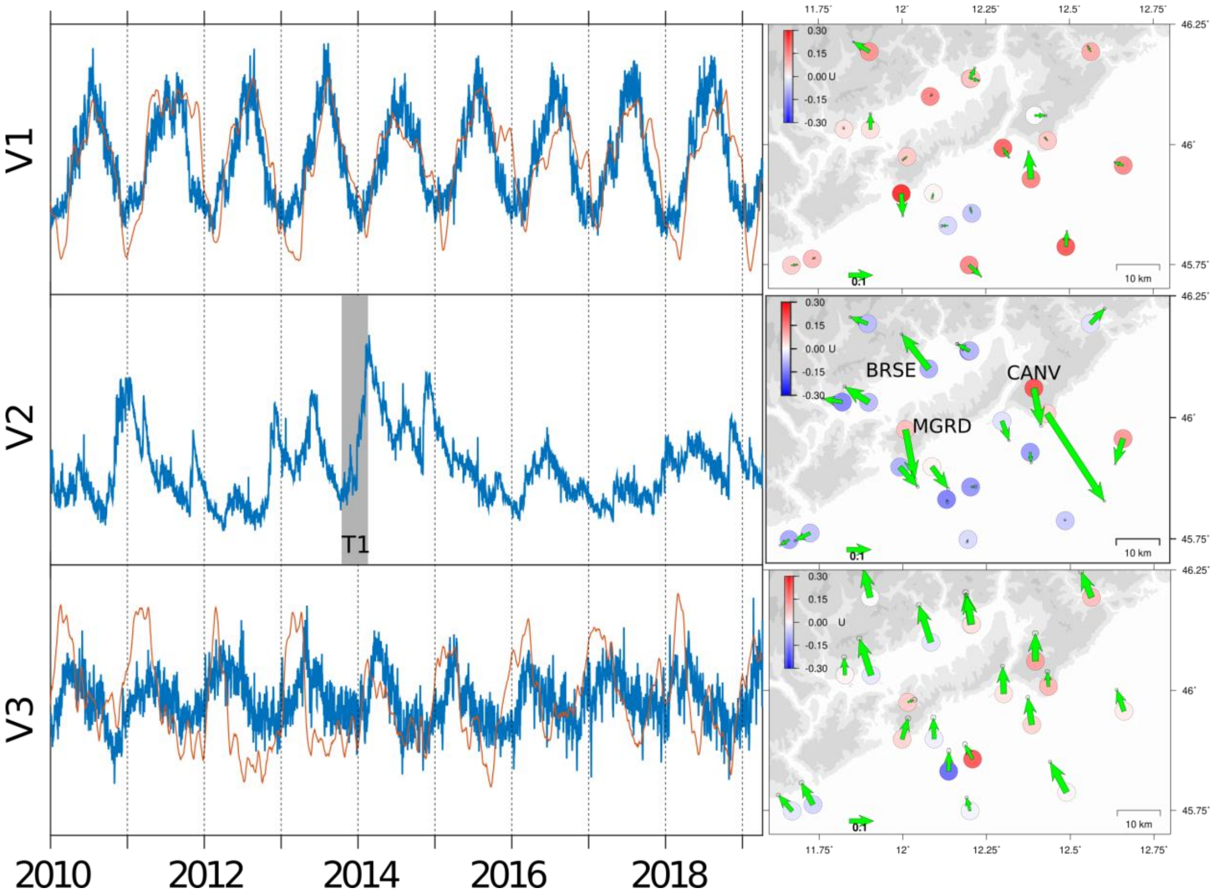

Figure 2. Temporal evolution (V; in blue) of the three ICs defined from the vbICA analysis and the corresponding spatial response in the horizontal (green arrows) and vertical (coloured circles) components, respectively. The gray area indicates the time interval (T1 = 10 October 2013 to 22 February 2014) for which ground displacements have been computed and shown in Fig. 3. The red lines superimposed to V1 and V3 represent the mean vertical and N-S displacements caused by surface mass loading, respectively, estimated from the ERA-interim (European Centre for Medium-Range Weather Forecasts, ECMWF reanalysis) model and provided by http://loading.u-strasbg.fr (Gegout et al., 2010).

3 Surface deformation and link with hydrology

Water redistribution on the continents implies several processes that cover a wide range of spatial and temporal scales. At scales larger than several hundreds of kilometers, GRACE satellite observations or land surface models, such as the GLDAS modeling platform (Rodell, 2016), can provide a fair estimate of TWS changes and are typically used to compute surface displacements (e.g, Craig et al., 2017). At local scale, ground-based observations such as soil moisture and groundwater head can describe storage and pore-pressure changes, but their spatial representativity is limited. At regional/meso-scale, water storage observations are rare. River discharge, for example, is representative over the drained area (i.e. catchment), but only represents one flux contributing to storage changes. In this work, we model meso-scale water storage changes using a model that is driven by meteorological river discharge observations.

Water storage changes in a downstream sub-catchment (see Supplementary Fig. S3) can be estimated based on the mass balance equation:

$$dS/dt = P + Qin - E - Qout - Qgw \quad (1)$$

where P, E, Qin, Qout, Qgw are respectively precipitation, actual evapotranspiration, incoming river inflow, outcoming river discharge, and potential groundwater import/export in a surrounding basin. Among the different water fluxes, P, Qin and Qout can be measured, whereas actual evapotranspiration and Qgw should be estimated with a model. It is worth noting that at regional scales (<100 km), lateral water fluxes could be significant, especially in a mountainous region, where the convergence of water from steep basins to valleys with gentle slopes favour transient accumulation of a large amount of water. Such lateral flow processes are hardly modeled within large-scale hydrological models.

The tool we use to estimate the right side factors of eq. 1 is the lumped parameter hydrological model GR5J (Pushpalatha et al., 2011), which allow us to quantify daily TWS changes at the scale of single hydrological basins (Fig. 3). The GR5J rainfall-runoff model is based on two storage compartments, which mimic the typical response of soils and groundwater to antecedent precipitation. This model is forced with precipitation, temperature and potential evapotranspiration and computes actual river discharge. It is typically calibrated on observed river discharge to define the eight mathematical parameters defining the dynamics of the two stores and their relations. The best set of parameters values is then defined by a Marquard-Levenberg least squares regression analysis using root mean square error on the logarithm of discharge as an objective function. As discharge vary over two orders of magnitude, calibrating the model on the logarithm of the discharge is preferred to ensure that both high and low flows have a similar weight. Finally, total water storage changes are computed as the sum of both stores.

The GR5J inputs are a daily value of precipitation, temperature and potential evapotranspiration; therefore, we estimate the precipitation and temperature value form 1 January 2010 to 31 March 31 2019 by computing a daily weighted mean of in-situ measurements provided by the Veneto Regional Agency for Environmental Prevention and Protection (ARPAV, http://www.arpa.veneto.it/bollettini/storico), using the Thiessen polygon method (Supplementary Text S2.1). Potential evapotranspiration has been evaluated by using the Jensen-Haise method (Jensen et al., 1990; Supplementary Text S2.2).

In the study area we define three hydrological basins by using the drainage direction maps (available on *www.hydrosheds.org/page/availability*) and watershed outlets located at the river discharge measurements on the Piave river at Belluno, Segusino and of the Cordevole river at Ponte Mas (see Fig. 3). The region of interest, though, is limited to a portion of a watershed located in the Belluno Valley. Considering the availability of river discharge data upstream and downstream this region, the model is calibrated and water storage changes computed on each of the watershed (Supplementary Text S2.3). The final TWS_{res} is set as the storage difference between the largest basin (Piave at Segusino) and its subbasins (Cordevole at Ponte Mas and the Piave at Belluno) as

$$TWS_{res}=TWS_{seg}-(TWS_{cor}+TWS_{bel}) \quad (2)$$

Where TWS_{seg}, TWS_{cor}, TWS_{bel} indicate the TWS computed in the Piave at Segusino, Cordevole at Ponte Mas and Piave at Belluno watersheds, respectively.

Fig. 4 shows that the normalized temporal evolution of the non-seasonal deformation signal (V2) and TWS_{res} are clearly correlated (Pearson correlation coefficient = 0.83), demonstrating that this transient deformation component is driven by changes in groundwater contents. The agreement is good both during (rapid) TWS_{res} increase and (slower) TWS_{res} decrease, either when small and/or slow TWS_{res} changes happen and during extreme events. This process is also displayed in Supplementary Movie S1.

On October 29th, 2018, storm Vaia, with >300 mm of cumulative precipitation in 72 hours and wind gusts exceeding 200 km/h, hit north-eastern Italy, causing the loss of 8 million cubic meters of standing trees. This extreme event is well recorded as a rapid increase of TWS_{res} (dashed line in Fig. 4) corresponding to extensional deformation recorded by the GNSS network, with the largest offsets at MGRD (~5 mm toward SE) and BRSE (~2.5 mm toward NW).

Figure 4 shows how EWT from GRACE and GRACE-FO measurements, processed at JPL using the Mascon approach (Version2/RL06, Watkins et al., 2015) is, as expected, overall less accurate in describing water storage changes at the scale of the hydrological basin studied in this work. As for TWS_{res}, EWT has ben detrended (linear trend= -1.04 cm/yr). Due to the sparse temporal sampling, EWT from GRACE misses most of the higher frequencies changes, resulting in a prevalent annual signal. Most importantly, it appears to be overall less accurate in representing the fast dynamics of a karst system in terms of changes in groundwater levels, as detected by the local hydrological model. This is likely due to the spatial resolution of GRACE measurements, which are prone to large errors when considering areas below 30,000 km^2 (Doumbia et al., 2019). As a consequence, GRACE data do not allow to identify rapid and localized water storage variations at the scale of the study area, being however useful to study hydrological processes at scales of mountain belts (Chen et al. 2018; Silverii et al., 2016).

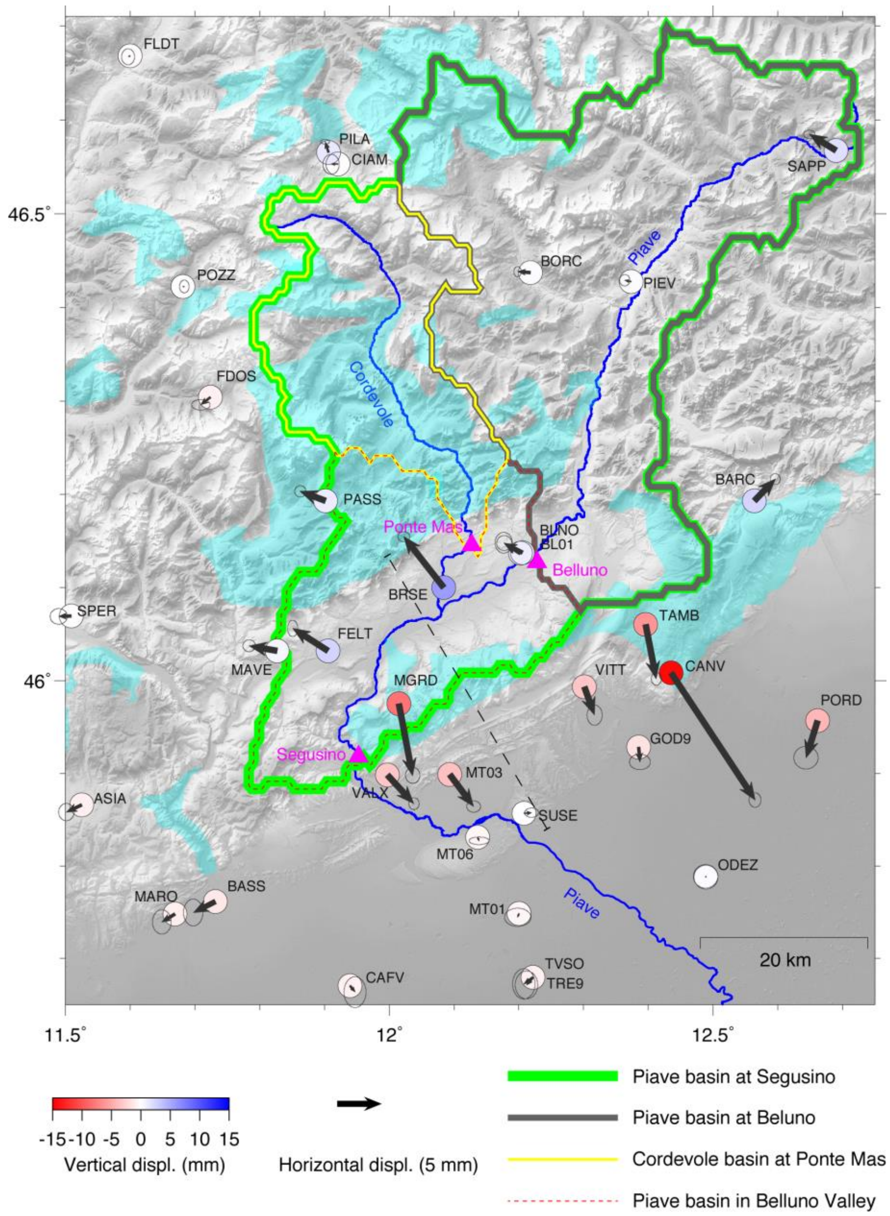

Figure 3. Hydrological map and geodetic displacements in the study region. Piave and Cordevole rivers (in blue) are gauged at three locations (purple triangles), defining three watersheds (yellow, green and grey) and the 883 km² region in-between (Belluno Valley, red dashed line) where water storage changes are modeled. Highly productive fissured karst aquifers are highlighted in cyan from the International Hydrogeological Map of Europe 1:1,500,000 (http://www.bgr.bund.de/ihme1500). Regional horizontal (black arrows) and vertical displacements (color dots), described by the second source of independent component analysis (IC2) on 67 GNSS stations during T1 period (winter 2013-2014) are superimposed (see also Fig. 2). The dashed black line show the trace of the geological cross section of Fig. 5.

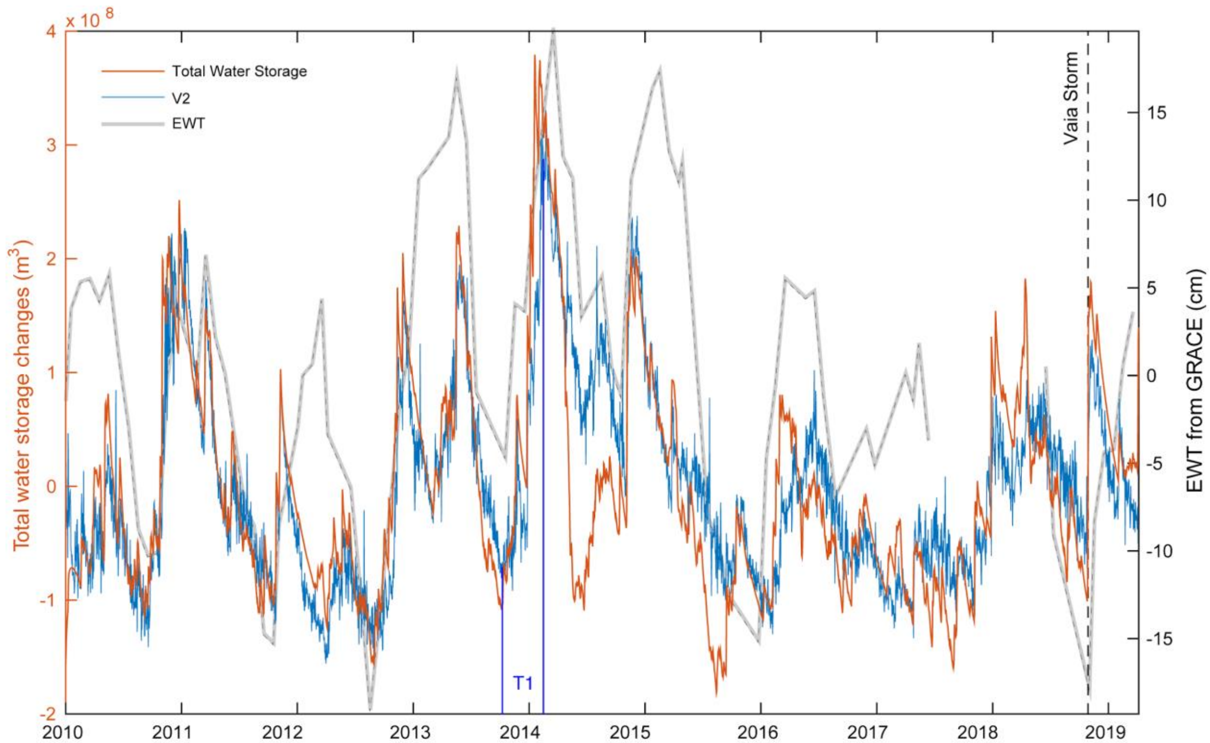

Figure 4. Temporal evolution of the modeled water storage changes in the Belluno Valley (orange, left axis), the geodetic IC2 (blue) and the EWT from GRACE and GRACE-FO measurements (gray). The linear trend of each curve has been removed (see Section 3). The blue vertical black lines indicate the T1 period and the vertical dashed line shows the epoch of the intense Vaia storm.

4 Surface deformation and link with geology

Transient displacements in the Alps have been interpreted as due to pressure changes associated with water level variations in vertical karst fractures (Devoti et al., 2015; Serpelloni et al., 2018). For the study area, Serpelloni et al. (2018) used a vertical tensile dislocation, in a homogeneous and uniform half space, showing that a similar structure is required to explain the horizontal displacements. However, the model proposed in Serpelloni et al. (2018) has limited relationships with the geology and hydrology of the area

In this work we develop a two-dimensional finite-element model (FEM) with the goal of testing different sources of deformation potentially able to accommodate groundwater level changes in the Belluno Valley, by comparing model results with the ground displacement pattern associated with IC2 (Fig. 2). The 2D model (the trace of the profile is shown as a discontinuous line in Fig. 3) is defined on the basis of the geological cross-section proposed by Galadini et al. (2005). We use the “Solid Mechanics” physics module of the COMSOL software (Supplementary Text S3.1), considering the problem as quasi-static at daily time scales and resolving the model as “stationary”. The model is constrained by geological and geophysical information and in agreement with both local seismicity (Danesi et al., 2015; Romano et al., 2019) and seismic prospections (Fantoni et al., 2002). The cross section is normal to the strike of the MCCV mountain range, that is almost parallel to the directions of geodetic displacements associated with IC2 (Fig. 2). We use data from the GNSS stations located within a distance of 20 km from the cross section (considering a length of ~40 km of the Belluno Valley), whose positions and

displacements are projected along the direction of the profile (Fig. 5). This analysis is focused on a specific time interval (10 October 2013 to 22 February 2014; T1 in Fig. 2 and Fig. 4), corresponding with a period of rapid increase of TWS_{res} and extensional deformation (Fig. 2).
The FEM model allows us to account for topography and subsurface geological features of the area, like the presence of faults and the different mechanical properties of the rock layers. The rock mechanical parameters used (Supplementary Table S2), in particular the Young modulus and Poisson's ratio, are taken from Anselmi et al. (2011).
Assuming that the pressure variations caused by the accumulation of water are directly proportional to the TWS_{res} changes, we test different models to describe the relation between TWS_{res} changes and the deformation associated with IC2 (Fig. 6). We consider two main families of water pressure distribution:
1) Models where pressure is distributed horizontally and applied vertically on the elastic domain: under this hypothesis, three models are tested: (i) the loading caused by water storage changes in an unconfined aquifer, hosted by the Belluno Basin Units, cause a downward pressure on the aquiclude (impermeable layer, here the Igne Formation) at the base of the aquifer (Model 1); (ii) We also take into account the possible role of the Bassano-Valdobbiadene back thrust (BVBT) and BVT faults as lateral aquiclude (Model 2); and (iii) we represent the surface loading on the Belluno Valley, assuming storage changes in a very shallow water reservoir, localized along the Piave river bed (Model 3).
2) Models where pressure is distributed vertically along sub-vertical structures and applied orthogonally in the modeled domain: under this hypothesis we test two models that mimic the impact of pressure changes in a single open fracture reaching the surface, which represents the network of fractured rocks in the damage-zone associated with the BVT (Model 4) and the BVBT (Model 5) faults. Fault damage zones in the carbonate rocks, in fact, often host open fractures (karst), demonstrating that they can also be conductive to fluid flow (Torabi et al., 2019). Transient pressure changes are applied on the whole fracture, following Longuevergne et al. (2009). Such behavior has been validated in fractured karstic systems in Lesparre et al. (2017).
We use two criteria to evaluate how well a model reproduce the displacements pattern associated with IC2 (Supplementary Fig. S10): the first is the ratio between vertical and horizontal displacement at each GNSS station, which should not significantly exceed 1; the second is the number of stations with the horizontal displacements pattern in agreement in sign with IC2. According to these criteria, the displacements pattern associated with IC2 is better reproduced by the models where pressure is distributed vertically than the ones where pressure is distributed horizontally. In fact the vertical displacements generated by the Models 1, 2 and 3 are too large compared to the horizontal ones, and the horizontal displacements pattern shows significant disagreement with the one associated with IC2 (Fig. 2). A detailed analysis of each tested model, in terms of fit of the horizontal and vertical displacements, can be found in the Supplementary Text S3.2.
The model that best reproduces the horizontal and vertical displacements is Model 5 (Fig. 6). Here the fracture is considered hydrologically conductive (Faulkner et al., 2010) down to 0 m a.s.l where it intersects an impermeable formation (the Igne Formation, see section 6.1 for details).
We finally analyse the influence of the topography and of the rock stratification on the result obtained by using Model 5. This test is performed by considering both the case where the topography is included but the domain is homogeneous (Model 5a), and the case of a

homogeneous domain with a flat free surface. We computed the horizontal and vertical displacements of the three models (Model 5b, Supplementary Fig. S11). We find that there is no significant difference among the three models (i.e., 5, 5a, and 5b) in reproducing the horizontal displacements. The vertical displacements generated by the two models in which the topography is included are very similar (Models 5 and 5a), but they differ from the results obtained using a model with a flat free surface (Model 5b). Nonetheless, since the noise level is higher in the vertical component than the horizontal one, the horizontal is considered as the most informative, as discussed in the Supplementary Text S3.2. Then, topography and layering do not significantly affect the horizontal displacements, while the vertical ones are more affected by the inclusion of the topography than the rock stratification.

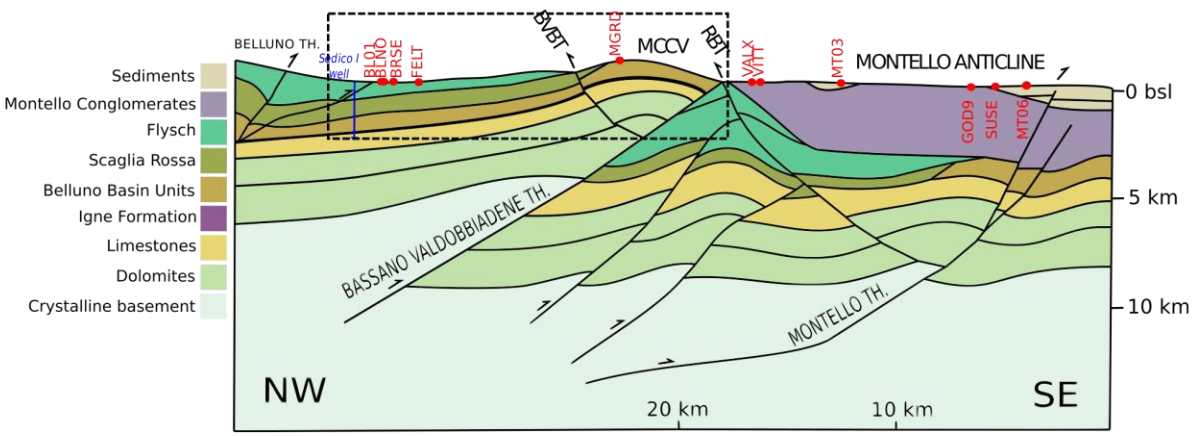

Figure 5. Geological cross section of the study area, modified from (Galadini et al., 2005); red dots: position of the GPS stations projected along this profile. RBT: Revine back thrust; BVBT: Bassano-Valdobbiadene back thrust. The dashed rectangle represents the area shown in Fig. 6.

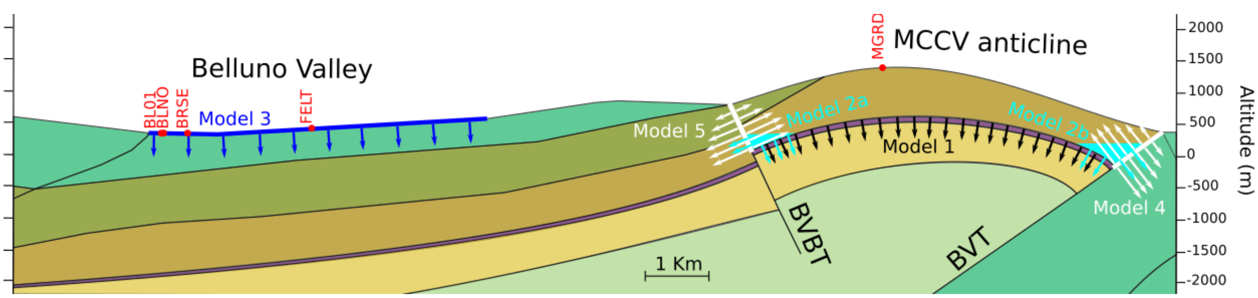

Figure 6. Zoom on the 2D model cross-section of Fig. 5, showing a schematic representation of the tested models used to explain the horizontal displacements reconstructed by IC2. MCCV: Mount Cesen-Col Visentin anticline; BVT: Bassano-Valdobbiadene thrust; BVBT: Bassano-Valdobbiadene back thrust. Rock formations are shown with the same legend of Fig. 5.

5 Studying the link between hydrology and seismicity

In Section 3 we demonstrate the link between changes in groundwater storage and surface deformation (Fig. 3) and in Section 4 we provide a physical model explaining this process, linked to the local geological features. In this section we investigate and test possible relationships between changes in TWS_{res} and seismicity rates. We use the local earthquake catalogue from Romano et al. (2019), which contains high-resolution relocations of 1609 events with magnitudes ranging from -0.8 to 4.5, in the period January 2012 to October 2017. This catalog was produced using data from the Collalto Seismic Network (Priolo et al., 2015) and represents one of the most accurate, high quality, earthquake catalogue for this sector of the Southern Alps.

Before exploring any possible link between seismicity rates and hydrological observations, first we calculate the completeness magnitude (Mc), obtaining a value Mc=0.7 for the full data set; the number of events above Mc is 731 (for details see Supplementary Text S4.1). Afterwards, we identify and remove the aftershock events that are more likely associated with earthquake stress-triggering processes. This analysis is performed by declustering the catalog in the time domain using the epidemic-type aftershock sequences model ETAS (Ogata, 1998). The resulting partition between background seismicity (372 events) and aftershocks (359 events) is presented in Fig. 7a. More details of this process are presented in the Supplementary Text S4.1. It is worth noting that, in the ETAS model, the background seismicity is assumed to be generated by a homogeneous Poisson process that is physically associated with a constant-rate tectonic loading process. However, the ETAS-based declustering process does not guarantee that the resulting background seismicity is actually stationary (Console et al., 2010); as a result, it is actually possible to observe temporal fluctuations in the background seismicity obtained after the temporal declustering process. This departure from stationarity is supposed to be caused by the temporal activation or quiescence of seismic sources forced by processes having a physical cause outside the stationary tectonic loading assumed by ETAS (Zhuang et al., 2002).

In this article we explore the presence of possible correlations between temporal variations in water storage observations, deformation and the background seismicity. With this aim, we adopt the covariate model proposed by Garcia-Aristizabal (2018), which allows us to perform a robust statistical evaluation of possible relationships between TWS_{res} changes (x_{TWS}) and background seismicity rates. This model has been previously used to study seismicity triggered by underground anthropogenic activity (as e.g., pressurized fluid injections, Garcia-Aristizabal 2018). The work presented in this article is the first application of this model to study correlations between seismicity and natural processes. According to Garcia-Aristizabal (2018), when the forcing process generating the seismicity in a given zone is stationary in time (as e.g., a constant tectonic loading), the background seismicity rates can be stochastically modelled using a homogeneous Poisson process; it implies that seismicity rates follow the Poisson distribution and, consequently, the times between consecutive events (inter-event times, t_{IET}) follow the exponential distribution. However, if the forcing process is non-stationary, and if it is possible to identify measurable parameters as *proxies* of the processes driving such non stationary behavior, then it is possible to model correlations between changes in seismicity rates and changes in the proxy parameters by linking them as covariates of the stochastic model parameters. In order to explore this possibility we set the exponential distribution as the basic template function for modelling the distribution of t_{IET}:

$$f\left(t_{IET} \vee \mu(x_{TWS})\right) = \frac{1}{\mu(x_{TWS})} exp\left(\frac{-t_{IET}}{\mu(x_{TWS})}\right) \qquad (3)$$

and the possible dependencies on hydrological data (in this case x_{TWS}) are modelled writing the μ parameter of the exponential distribution in terms of deterministic functions of x_{TWS} of the explanatory covariate (Supplementary Text S4.3). x_{TWS} is measured respect to a reference TWS_{res}

assumed to be the minimum value reached by this parameter in the analysed period. We hypothesize that seismicity rates observed in this zone may be the result of the superposition of a constant rate due to tectonic loading and a seismicity rate perturbation caused by hydrologically-driven stress changes. With this aim we test polynomial functions relating $log(\mu)$ and x_{TWS} as follows:

$$log[\mu(x_{TWS})] = \sum_{j=0}^{n} \alpha_j (x_{TWS})^j \quad (4)$$

where $\alpha_j = (\alpha_1, \alpha_2, \ldots, \alpha_n)$ is a vector of coefficients of the polynomial function relating the μparameter of the exponential distribution with the selected covariate x_{TWS}. We study in particular two competing models: 1) the case $n = 0$, representing a stationary model (i.e., non dependence on x_{TWS}, and therefore the seismicity rates mainly associated to tectonic loading), and 2) the case $n = 1$, representing a log-linear relationship (that is, an exponential relationship between μ and x_{TWS}), which represents the case of seismicity rate resulting from constant tectonic loading modulated by the hydrological processes described by x_{TWS}. The input data are pairs of t_{IET} and the respective x_{TWS} averaged in a Δt time window (for which we test different values ranging from days to weeks). The inference of model parameter values is performed using a Markov chain Monte Carlo method, and the selection of the preferred model is performed calculating the Bayes factor, B_{KL} (Garcia-Aristizabal, 2018). B_{KL} summarizes the evidence provided by the data in favour of one specific model (K) as opposed to another (L), i.e. $B_{KL} < 1$ supports the reference model (L), whereas $B_{KL} > 1$ supports the K competing model (the higher the value, the more evidence in favor of K). Reference values for interpreting B_{KL} have been provided by Jeffreys (1961) and Raftery (1995) and are summarized in Supplementary Table S4 in the Supplementary Text S4.3.

The seismicity in the study area is mainly generated as a result of the Adria-Eurasia plate convergence process, accommodated by different, sub-parallel, thrust faults (Fig. 1). In order to quantitatively identify possible spatial sets of seismicity (possibly related to different seismotectonic features) we implement a cluster analysis in the spatial domain (Supplementary Text S4.2) using the k-means algorithm (MacQueen, 1967); the optimum partition is selected using the Silhouette approach (Rousseeuw, 1987). We find that the background seismicity can be partitioned into two main clusters (Fig. 7b): (i) cluster A (orange points), composed by 154 events located in the SW part of the domain, where earthquakes can be associated with the Montello thrust and the BVT faults (Danesi et al., 2015); (ii) cluster B (blue points), composed by 218 events located in the NE part of the domain, in which most of the seismicity can be associated with the N-dipping Cansiglio thrust fault (Galadini et al., 2005; Fig. 1b). This preferential cluster partitioning roughly reflects the two main features that we observe in the spatial distribution of the seismicity (Fig. 7a): a set of events mostly grouped in the NE part, and a more evenly distributed seismicity towards the SW.

The correlation analysis using the covariate approach is then performed using the data from each spatial cluster of background seismicity. The parameter values of the fitted models are summarized in the Supplementary Table S6. Comparing plots of the moving average of both TWS_{res} and the rate of seismic events (calculated in 90-days length time windows sliding at increments of 1 day) for cluster A (Fig. 8a) and cluster B (Fig. 8b), we observe that only the seismicity rate in cluster A tends to change in agreement with the changes in the TWS_{res}. This observation is quantitatively confirmed by the covariate analysis (Supplementary Text S4.3), with the B_{KL} indicating that only for cluster A the non stationary model performs better than the alternative stationary solution (Supplementary Table S5). In fact, for cluster A (i.e., the seismicity associated with the Montello thrust and the BVT faults) there is positive evidence ($B_{KL} = 5.24$) supporting a log-linear relationship between the seismicity rate (modelled through the distribution of inter-event times, t_{IET}) and the TWS_{res} changes, in contrast to a stationary reference model (Fig. 8c). For cluster B, the evidence supports the stationary model (B_{KL}= 0.57, Fig. 8d), indicating a not significant (or not identifiable) link between seismicity rates in the Cansiglio thrust fault zone and TWS_{res} changes in the Belluno Valley. It is worth noting that our analysis do not identify a link between TWS_{res} and the seismicity rates in cluster B. We cannot discern whether this result is related to an actual missing link between these two processes or a consequence of limitations in both methods and available data. In our opinion, both possibilities are plausible. A reasonable explanation for an eventual missing link between these two processes is that cluster B is located relatively far from the modeled source of deformation; consequently, the magnitude of the stress perturbation for this area (caused by the modeled deformation source) is smaller than the stress perturbation in the zone where cluster A is located (which is closer to the deformation source).

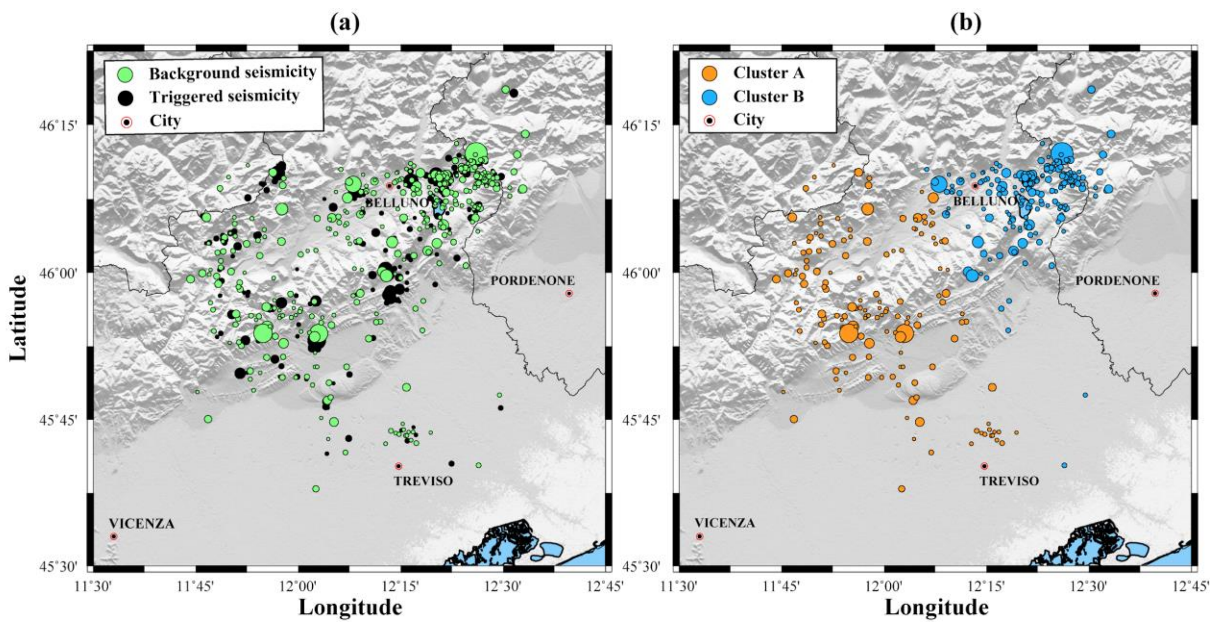

Figure 7. (a) Seismicity in the study area, separated as background (green circles) and triggered (black circles) seismicity according to the ETAS model. **(b)** Clusters (A and B) of background seismicity identified using spatial cluster analysis.

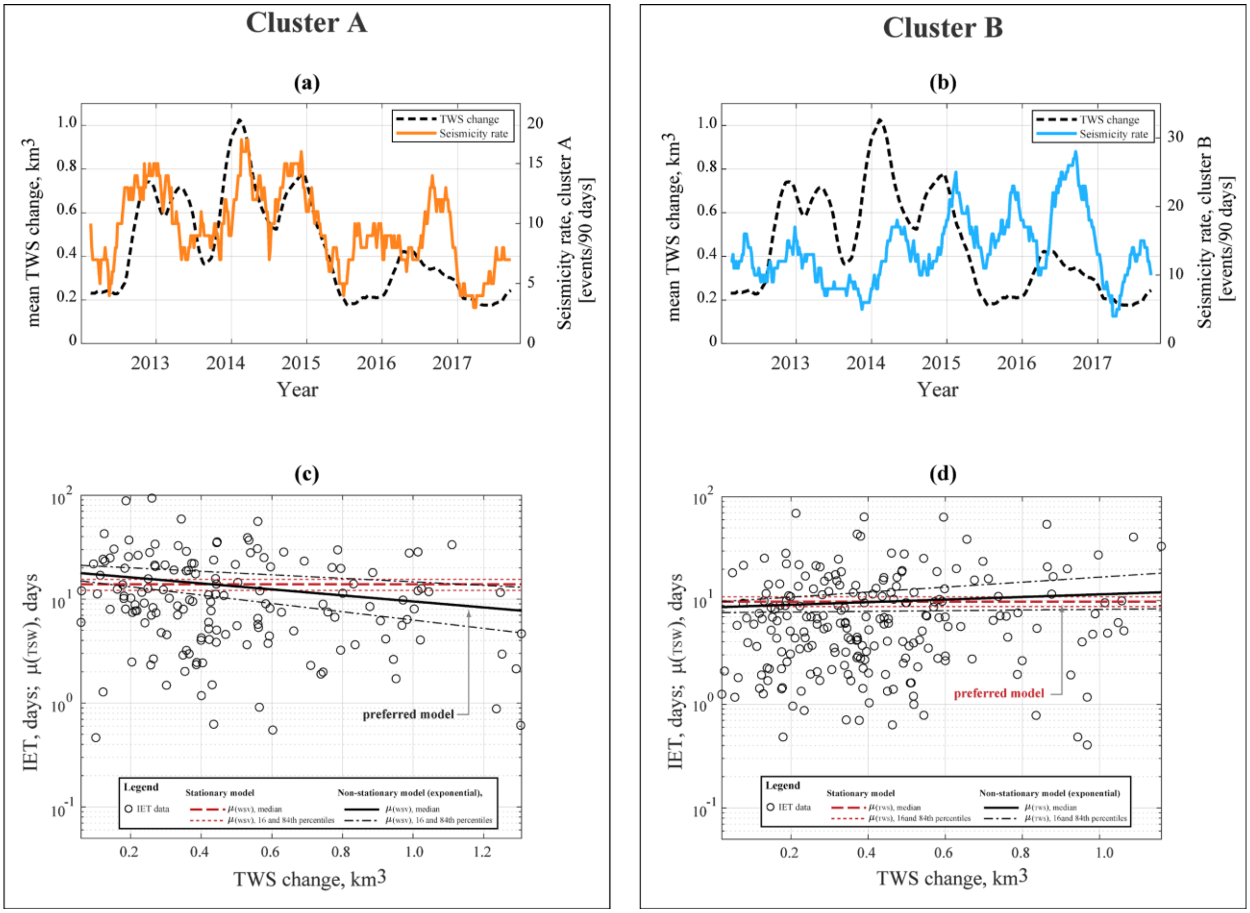

Figure 8. Moving average TWS (discontinuous black) and rate of seismic events in **(a)** cluster A (continuous orange) and **(b)** cluster B (continuous blue), calculated in 90-days length time windows sliding at increments of 1 day. Plot of inter-event times in **(c)** cluster A and **(d)** cluster B against TWS changes, and the results for the two tested models: stationary model (red) and Log-linear (black). Preferred models are indicated with the arrow in (c) (d).

6 Discussion

6.1 Hydromechanical coupling

In Sections 3 and 4 we describe the link between hydrological processes and solid Earth deformation by the joint interpretation of results from hydrological and mechanical models constrained by geodetic, hydrological, meteorological observations and geological/geophysical information on subsurface structural and tectonic settings. The high ratio between horizontal and vertical displacements (Supplementary Fig. S10), suggests that the most likely mechanism able to produce the horizontal, anisotropic, extensional deformation, observed during a phase of large water storage increase, is the water accumulation in narrows, subvertical, geological structures. The same mechanism is assumed to be able to explain smaller deformation associated with phases of smaller TWS_{res} increase, and, with inverted sign, to explain the observed compressional deformation during phases of TWS_{res} decrease, responding to the fast dynamics of karst systems, including extreme events (e.g., the 2018 Vaia storm).
We identify the back thrust associated with the Bassano-Valdobbiadene thrust fault as the main source of deformation. We assume that the network of damage-zone faults, which is modeled as a single fracture associated with BVBT (i.e., Model 5), are well connected and water-saturated

and the water level varies as the TWS_{res}, causing pressure changes orthogonal to fracture walls. It is likely that the water feeding the fracture mainly comes from the top of the MCCV mountain chain: the higher fracture density at the hinge zone of the anticline (e.g., Feng and Gu, 2017) and the well-developed epikarst in the exposed rock formations (Maiolica and Rosso Ammonitico) suggest the presence of an epikarst circulation on the top of MCCV chain (Klimchouk and Sauro, 1996). The combined effect of the epikarst and the presence of a shallow, low permeable layer (the Fonzaso formation, located at ~200 m of depth from the surface) facilitates the rapid infiltration of precipitation water and its flow toward the back thrust, following the northward inclination of rock layers and stratification. This hypothesis is supported by the observed lack of a time-delay, at the daily time scale, between TWS_{res} and the geodetic deformation signal (Fig. 4). However, we can not exclude that water can flow southward, toward the BVT, which might behave similarly to the back thrust as an hydrologically active structure, at lower dip (Supplementary Text S3.2, Model 4). Nonetheless, the site MGRD (Fig. 1a) moves toward the BVT and away from the back thrust when TWS_{res} increases, implying that the role of the 30° dipping BVT, as hydrologically active structure, is likely to have a secondary effect with respect to its back thrust.

A more precise description of the source of deformation, which includes the identification of both the fracture bottom position and the water level rise inside it, is not straightforward because of the trade-off between fracture width and its opening (e.g., Devoti et al., 2015; Silverii et al., 2016). Because of the lack of evidences of aquifers reaching depths that are hundreds of meters below the sea level surface, and since the maximum water level variation measured in a similar karst system is ~300 m (Milanovic, 2005), we assume the bottom position of the fracture at 0 m above sea level, at the interface between the Vajont limestone and the more impermeable Igne formation (see Fig. 6). Once set the bottom position of the fracture, the water level rise providing the best match between modeled and observed displacements is 100 m (Supplementary Fig. S10); this water level inside the fracture is located at about 10 m below the free surface when V2 reaches its maximum during the analyzed time-period (i.e., January, 2014). Furthermore, we analyze the effect of the initial opening of the fracture when applying the same pressure values on its walls, finding that assuming different initial opening values does not impact significantly the resulting displacements (Supplementary Fig. S12). As a consequence, the volumes of water involved cannot be quantified, since the only quantity affecting the displacements is the water level variation, while the initial fracture opening does not play a key role.

Given the spatial distribution and density of available geodetic data, the 2D numerical model used in this work can be considered as an acceptable simplification. However, we are aware of its limitations. We are assuming that geological features (including, for example, outcropping formations, fracture spacing, strike of faults and fractures, topography) are constant along the SW-NE direction, for about 40 km, which is not necessarily true. A 2D model cannot take into account the fact the the MCCV mountain chain and associated thrust and back thrust faults curve north, going into the N-S trending Fadalto valley (see Fig. 1). More importantly, changes in water level along the back thrust are implicitly assumed to be uniform along its strike in a 2D model, but an heterogeneous change in water level can cause more localized deformation signals, which would be however difficult to detect with the present GNSS network configuration. Moreover, effects associated with similar processes occurring at nearby karst systems cannot be taken into consideration. Hydrological deformation in the Cansiglio plateau, in fact (Devoti et al., 2015; Serpelloni et al., 2018) may affect GNSS sites VITT and GOD9 (Fig. 1).

6.2 Seismotectonic implications

Two main mechanisms have been suggested to explain hydrological modulation of seismicity: variations in pore-fluid pressure at hypocentral depths (Hainzl et al., 2006) and direct stress on the fault plane (Bettinelli et al., 2008; Craig et al., 2017; D'Agostino et al., 2018; Johnson et al., 2017). In the latter case, there is usually a little or no time delay between hydrological indicators and seismicity rate. In the former, seismicity rate variations are usually delayed with respect to hydrological observations by a time lag, which is strictly dependent on the earthquake nucleation depth and on the hydraulic diffusivity of the material between the surface and the seismicity source. The lack of temporal delay between the seismicity rate and the TWS_{res} (Fig. 8a) excludes an important role for poroelastic contributions, making the direct effect of stress changes at seismogenic depths the most likely process linking hydrology and seismicity.

In case of seasonal stress perturbations, seismicity rates can correlate either with the stress values or with stress rates, depending if the period of the stress perturbation (T_p) is smaller or larger than a critical period (T_a), which in turn is controlled by the loading plate velocity (Ader et al., 2014). The period that dominates the temporal evolution of stress in the study area is 1 yr (Supplementary Fig. S7), which is a value that T_a reaches only in rapidly deforming regions (Bettinelli et al., 2008). In slowly deforming regions, such as the Southern Alps, T_a usually assumes larger values. This observation is consistent with our findings, implying that stress changes are proportional to the magnitude of the TWS_{res} and not to its time derivative (which represents whether TWS_{res} is in an increasing or decreasing phase).

We estimate the stress change associated with the deformation caused by the water pressure increase (T1 time window in Fig. 4) in the hypothesized fracture source. In practice, we calculate the Coulomb failure function (CFF, Supplementary Text S3.3) on receiving planes oriented in agreement with the compressional tectonic regime of the area. Fig. 9a shows CFF values obtained assuming a shallow-dipping (10°) decollement (i.e. the Montello flat) as receiving source, showing that in the depth interval where most of the seismicity associated with cluster A (see Fig. 7b) is located (4-14 km), positive stress changes may be as large as 25 kPa. These stress changes are larger than stressing rates from tectonic loading, which are expected to be of the order of 1-3 kPa/yr (Caporali et al., 2018). Similar values are obtained, but with different spatial patterns, assuming different thrust-receiving sources; however, a spatial correlation between areas of stress increase and background seismicity is not evident. However, it is worth considering that the faulting mechanisms of the background seismicity are not well constrained, and the focal mechanisms available for the events in the catalogue of Romano et al. (2019), or other studies (e.g., Anselmi et al., 2011), show a large range of mechanisms, including normal, thrust and strike-slip faulting on different planes. Therefore, while a clear spatial correlation between seismicity and regions of positive stress increase is not apparent, it is likely that the highly deformed upper crust, inherited by the complex tectonic evolution of the Southern Alps (Castellarin and Cantelli, 2000), provides heterogeneous response to the hydrologically-modulated stress changes. Another important factor possibly playing a role in the apparent missing fit between seismicity locations and stress increase are the uncertainties in earthquake locations. Uncertainties in the location of small earthquakes are usually large; the formal errors reported with earthquake locations are mostly based on uncertainties on seismic-phase arrival time measurements that in general give unrealistic small mislocation errors respect to what is observed when other sources of uncertainty (as e.g. modelling errors related to travel time calculations and the nonlinearity of the location problem) are considered (see e.g., Garcia-Aristizabal et al. 2020).

It is however important to note that the amplitude of the CFF field generated by the TWS_{res} increase in hydrologically active fracture is much larger than the one generated by the annual surface hydrological mass loading (Fig. 9b), which actually is considered as the main mechanisms that modulate seismicity rates in other regions (Hainzl et al., 2014; Johnson et al., 2017), where much greater annual vertical displacements, and consequently greater seasonal stress perturbations than those observed in the Alps, are present. We finally point out that, as shown in Supplementary Fig. S13, the topography and geological features of the domain do not significantly affect the CFF patterns.

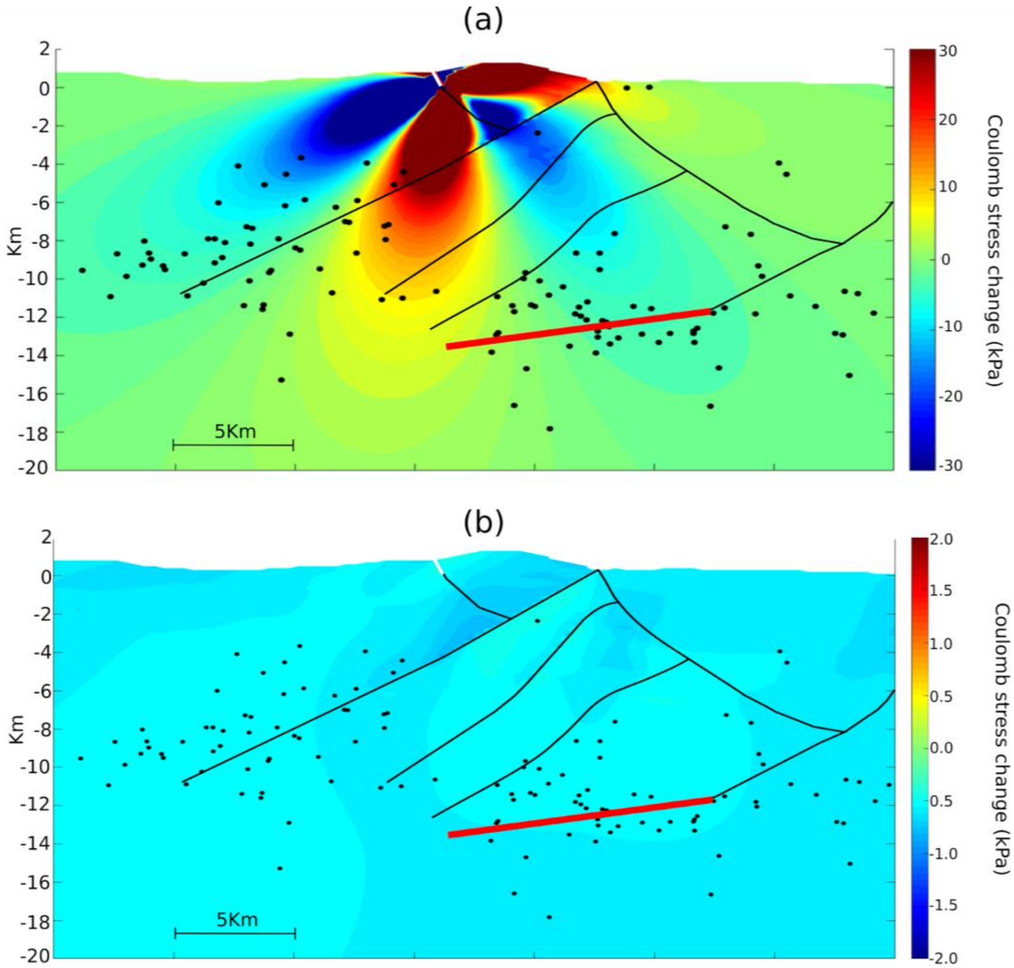

Figure 9. (a) Coulomb stress change during a phase of TWS_{res} increase (T1 in Fig. 4) caused by a source of deformation as in Model 5 (see Supplementary Text S3.2), considering planes parallel to the Montello decollement (dip angle=10°), highlighted in red. **(b)** Coulomb stress change calculated on the same dipping planes considering as source of deformation a 1 kPa uniform load on the free surface. This value causes a subsidence of ~3.8 mm, which is consistent with the amplitude of the vertical displacements caused by the large scale superficial loading in the time interval that goes from summer to winter (see Fig. 2) and inhibits thrust faulting (negative CFF values in all the domain). The black dots represent the background seismicity of cluster A.

7 Conclusions

Using geodetic and environmental data, integrated into hydrological and mechanical models, we show how water convergence toward a specific zone, can generate horizontal surface displacements that are superimposed to annual surface hydrological loading and horizontal, linear, tectonic loading. We find that the background seismicity of a spatial cluster distributed across the fold-and-thrust belt is correlated with the temporal evolution of water storage changes. Although the limited spatial and temporal extent of the earthquake catalogue will require future analyses to support this conclusion. Hydraulic pressure changes in a shallow hydrologically active fracture (<1 km) can generate large shears (~10 kPa) in faults oriented orthogonally and at distances of the order of ~10 km (horizontally and vertically). A highly deformed upper crust may be responsible for an heterogeneous response to the hydrologically-modulated stress changes. The link between hydrology, deformation and seismicity may be favoured by 1) the existence of a (shallow) hydrologically-active fracture connected to the surface, 2) water convergence from a watershed/river basin towards the hydrologically active structure, leading to large water storage (and therefore water pressure) changes and 3) the existence of properly oriented (orthogonal), seismically active structures (such as a classical thrust/back thrust couple). In such contexts, horizontal deformation is best suited to highlight physical links between surface deformation and hydro-mechanical processes occurring at depth.

Acknowledgements

We thank L. Anderlini for helpful discussions and suggestions on stress analysis and E. Scoccimarro for suggestion on the analysis of pluviometric data.

Competing interests

The authors declare no competing interests.

Data availability

Precipitation, temperature and river flow data are provided by "Agenzia Regionale per la Prevenzione e Protezione Ambientale del Veneto" (ARPAV): https://www.arpa.veneto.it/bollettini/storico/Mappa_2019_TEMP.htm.

Extraterrestrial irradiance data are available from http://www.soda-pro.com/web-services/radiation/extraterrestrial-irradiance-and-toa.

Drainage direction maps used to define river basins are available on www.hydrosheds.org/page/availability.

The analyzed seismic catalog is available in the supplementary material of Romano et al. (2019).

We use publicly available raw GNSS data. However, RINEX data can be requested to E.S., if not yet available on the original repositories.

Raw GPS time series are available on https://doi.org/10.1594/PANGAEA.912895

The Collalto Seismic Network data are available on https://doi.org/10.7914/SN/EV.

GRACE EWT data: D. N. Wiese, D.-N. Yuan, C. Boening, F. W. Landerer, M. M. Watkins. 2019. JPL GRACE and GRACE-FO Mascon Ocean, Ice, and Hydrology Equivalent Water

Height JPL Release 06 Version 02. Ver. 2. PO.DAAC, CA, USA. Data set accessed [2020-04-29] at https://doi.org/10.5067/TEMSC-3MJ62.

Code availability

The MATLAB code for TWS estimation and vbICA decomposition are available from the corresponding author on request.

Founding source

This work and F. Pintori are supported by the project TRANSIENTI, founded by the Italian Ministry of Education, Universities and Research (MIUR) "Premiale 2014".

References

Ader, T.J., Lapusta, N., Avouac, J.-P. & Ampuero, J.-P. (2014). Response of rate-and-state seismogenic faults to harmonic shear-stress perturbations. *Geophysical Journal International*, 198, 385–413. https://doi.org/10.1093/gji/ggu144

Anderlini, L., Serpelloni, E., Tolomei, C., De Martini, P.M., Pezzo, G., Gualandi, A., & Spada, G. (2020). New insights into active tectonics and seismogenic potential of the Italian Southern Alps from vertical geodetic velocities. https://doi.org/10.5194/se-2020-10

Anselmi, M., Govoni, A., De Gori, P. & Chiarabba, C. (2011). Seismicity and velocity structures along the south-Alpine thrust front of the Venetian Alps (NE-Italy). *Tectonophysics,* 513, 37–48. https://doi.org/10.1016/j.tecto.2011.09.023

Bettinelli, P., Avouac, J.-P., Flouzat, M., Bollinger, L., Ramillien, G., Rajaure, S., & Sapkota, S. (2008). Seasonal variations of seismicity and geodetic strain in the Himalaya induced by surface hydrology. *Earth and Planetary Science Letters,* 266, 332–344. https://doi.org/10.1016/j.epsl.2007.11.021

Borsa, A.A., Agnew, D.C., & Cayan, D.R. (2014). Remote Hydrology. Ongoing drought-induced uplift in the western United States. *Science,* 345, 1587–1590. https://doi.org/10.1126/science.1260279

Caporali, A., Braitenberg, C., Montone, P., Rossi, G., Valensise, G., Viganò, A., & Zurutuza, J. (2018). A quantitative approach to the loading rate of seismogenic sources in Italy. *Geophysical Journal International,* 213, 2096–2111. https://doi.org/10.1093/gji/ggy112

Castellarin, A., & Cantelli, L. (2000). Neo-Alpine evolution of the Southern Eastern Alps. *Journal of Geodynamics*, 30, 251–274. https://doi.org/10.1016/S0264-3707(99)00036-8

Chanard, K., Avouac, J.P., Ramillien, G., & Genrich, J. (2014). Modeling deformation induced by seasonal variations of continental water in the Himalaya region: Sensitivity to Earth elastic structure. *Journal of Geophysical Research: Solid Earth*, 119, 5097–5113. https://doi.org/10.1002/2013JB010451

Chanard, K., Fleitout, L., Calais, E., Barbot, S., & Avouac, J.-P. (2018). Constraints on transient viscoelastic rheology of the asthenosphere from seasonal deformation. *Geophysical Research Letters*, 45, 2328–2338. https://doi.org/10.1002/2017GL076451

Chan, K., Lee, T.-W., & Sejnowski, T.J. (2003). Variational Bayesian Learning of ICA with Missing Data. *Neural Computation*, 15, 1991–2011. https://doi.org/10.1162/08997660360675116

Chen, W., Braitenberg, C., & Serpelloni, E. (2018). Interference of tectonic signals in subsurface hydrologic monitoring through gravity and GPS due to mountain building. *Global and Planetary Change*, 167, 148-159. https://doi.org/10.1016/j.gloplacha.2018.05.003

Console, R., Jackson, D.D., & Kagan, Y.Y. (2010). Using the ETAS model for catalog declustering and seismic background assessment. *Pure and Applied Geophysics,* 167, 819–830. https://doi.org/10.1007/s00024-010-0065-5

Craig, T.J., Chanard, K., Calais, E. (2017). Hydrologically-driven crustal stresses and seismicity in the New Madrid Seismic Zone. *Nature Communications*, 8, 2143. https://doi.org/10.1038/s41467-017-01696-w

D'Agostino, N., Silverii, F., Amoroso, O., Convertito, V., Fiorillo, F., Ventafridda, G., & Zollo, A. (2018). Crustal deformation and seismicity modulated by groundwater recharge of karst aquifers. *Geophysical Research Letters*, 45, 12,253-12,262. https://doi.org/10.1029/2018GL079794

Danesi, S., Pondrelli, S., Salimbeni, S., Cavaliere, A., Serpelloni, E., Danecek, P., Lovati, S., & Massa, M. (2015). Active deformation and seismicity in the Southern Alps (Italy): The Montello hill as a case study. *Tectonophysics*, 653, 95–108. https://doi.org/10.1016/j.tecto.2015.03.028

Devoti, R., Riguzzi, F., Cinti, F.R., & Ventura, G. (2018). Long-term strain oscillations related to the hydrological interaction between aquifers in intra-mountain basins: A case study from Apennines chain (Italy). *Earth and Planetary Science Letters*, 501, 1–12. https://doi.org/10.1016/j.epsl.2018.08.014

Devoti, R., Zuliani, D., Braitenberg, C., Fabris, P., & Grillo, B. (2015). Hydrologically induced slope deformations detected by GPS and clinometric surveys in the Cansiglio Plateau, southern Alps. *Earth and Planetary Science Letters*, 419, 134–142. https://doi.org/10.1016/j.epsl.2015.03.023

Doumbia, C., Castellazzi, P., Rousseau, A. N., & Amaya, M. (2019). High Resolution Mapping of Ice Mass Loss in the Gulf of Alaska From Constrained Forward Modeling of GRACE Data. *Frontiers in Earth Science*, 7, 360. https://doi.org/10.3389/feart.2019.00360

Drouin, V., Heki, K., Sigmundsson, F., Hreinsdóttir, S., & Ófeigsson, B.G. (2016). Constraints on seasonal load variations and regional rigidity from continuous GPS measurements in Iceland, 1997–2014. *Geophysical Journal International,* 205, 1843–1858. https://doi.org/10.1093/gji/ggw122

Famiglietti, J.S., Lo, M., Ho, S.L., Bethune, J., Anderson, K.J., Syed, T.H., Swenson, S.C., de Linage, C.R., & Rodell, M. (2011). Satellites measure recent rates of groundwater depletion in California's Central Valley. *Geophysical Research Letters,* 38. https://doi.org/10.1029/2010GL046442

Fantoni, R., Catellani, D., Merlini, S., Rogledi, S., & Venturini, S. (2002). La registrazione degli eventi deformativi cenozoici nell'avampaese Veneto-Friulano. *Mem. Soc. Geol. It* 57, 301–313.

Faulkner, D.R., Jackson, C.A.L., Lunn, R.J., Schlische, R.W., Shipton, Z.K., Wibberley, C.A.J., Withjack, M.O. (2010). A review of recent developments concerning the structure, mechanics and fluid flow properties of fault zones. *Journal of Structural Geology*, 32, 1557–1575. https://doi.org/10.1016/j.jsg.2010.06.009

Feng, J., & Gu, K. (2017). Geomechanical Modeling of Stress and Fracture Distribution during Contractional Fault-Related Folding. *Journal of Geoscience and Environment Protection*, 05, 61–93. https://doi.org/10.4236/gep.2017.511006

Filippini, M., Squarzoni, G., De Waele, J., Fiorucci, A., Vigna, B., Grillo, B., Riva, A., Rossetti, S., Zini, L., Casagrande, G., Stumpp, C., Gargini, A. (2018). Differentiated spring behavior under changing hydrological conditions in an alpine karst aquifer. *Journal of hydrology*, 556, 572–584. https://doi.org/10.1016/j.jhydrol.2017.11.040

Fu, Y., Argus, D.F., Freymueller, J.T., & Heflin, M.B. (2013). Horizontal motion in elastic response to seasonal loading of rain water in the Amazon Basin and monsoon water in Southeast Asia observed by GPS and inferred from GRACE. *Geophysical Research Letters*, 40, 6048–6053. https://doi.org/10.1002/2013GL058093

Galadini, F., Poli, M.E., & Zanferrari, A. (2005). Seismogenic sources potentially responsible for earthquakes with $M \geq 6$ in the eastern Southern Alps (Thiene-Udine sector, NE Italy). *Geophysical Journal International*, 161, 739–762. https://doi.org/10.1111/j.1365-246X.2005.02571.x

Garcia-Aristizabal, A. (2018). Modelling fluid-induced seismicity rates associated with fluid injections: examples related to fracture stimulations in geothermal areas. *Geophysical Journal International*, 215, 471–493. https://doi.org/10.1093/gji/ggy284

Garcia-Aristizabal, A., Danesi, S., Braun, T., Anselmi, M., Zaccarelli, L., Famiani, D., & Morelli, A. (2020). Epistemic Uncertainties in Local Earthquake Locations and Implications for Managing Induced Seismicity. *Bulletin of the Seismological Society of America.* https://doi.org/10.1785/0120200100

Gegout, P., Boy, J.P., Hinderer, J., & Ferhat, G. (2010). Modeling and Observation of Loading Contribution to Time-Variable GPS Sites Positions, in: *Mertikas, S.P. (Ed.), Gravity, Geoid and Earth Observation: IAG Commission 2: Gravity Field, Chania, Crete, Greece, 23-27 June 2008, International Association of Geodesy Symposia.* Springer Berlin Heidelberg, Berlin, Heidelberg, pp. 651–659. https://doi.org/10.1007/978-3-642-10634-7_86

Gualandi, A., Nichele, C., Serpelloni, E., Chiaraluce, L., Anderlini, L., Latorre, D., Belardinelli, M.E., & Avouac, J.P. (2017a). Aseismic deformation associated with an earthquake swarm in the northern Apennines (Italy). *Geophysical Research Letters,* 44, 7706–7714. https://doi.org/10.1002/2017GL073687

Gualandi, A., Perfettini, H., Radiguet, M., Cotte, N., Kostoglodov, V. (2017b). GPS deformation related to the *Mw* 7.3, 2014, Papanoa earthquake (Mexico) reveals the aseismic behavior of the Guerrero seismic gap. *Geophysical Research Letters,* 44, 6039–6047. https://doi.org/10.1002/2017GL072913

Gualandi, A., Serpelloni, E., & Belardinelli, M.E. (2016). Blind source separation problem in GPS time series. *Journal of Geodesy*, 90, 323–341. https://doi.org/10.1007/s00190-015-0875-4

Hainzl, S., Aggarwal, S.K., Khan, P.K., & Rastogi, B.K. (2014). Monsoon-induced earthquake activity in Talala, Gujarat, India. *Geophysical Journal International*, 200, 627–637. https://doi.org/10.1093/gji/ggu421

Hainzl, S., Kraft, T., Wassermann, J., Igel, H., & Schmedes, E. (2006). Evidence for rainfall-triggered earthquake activity. *Geophysical Research Letters,* 33. https://doi.org/10.1029/2006GL027642

Jensen, M.E., Burman, R.D., & Allen, R.G., (1990). Evapotranspiration and irrigation water requirements. ASCE Manuals and Reports on Engineering Practices No. 70., American Society of Civil Engineers, New York, NY, 360 p.

Johnson, C.W., Fu, Y., & Bürgmann, R. (2017). Seasonal water storage, stress modulation, and California seismicity. *Science,* 356, 1161–1164. https://doi.org/10.1126/science.aak9547

Klimchouk, A.B., & Sauro, U. (1996). “Hidden” shafts at the base of the epikarstic zone: a case study from the Sette Communi plateau, Venetian Pre-Alps, Italy. *Cave and karst science,* 23, 101–107.

Lesparre, N., Boudin, F., Champollion, C., Chéry, J., Danquigny, C., Seat, H.C., Cattoen, M., Lizion, F., & Longuevergne, L. (2017). New insights on fractures deformation from tiltmeter data measured inside the Fontaine de Vaucluse karst system. *Geophysical Journal International*, 208, 1389–1402. https://doi.org/10.1093/gji/ggw446

Longuevergne, L., Florsch, N., Boudin, F., Oudin, L., & Camerlynck, C. (2009). Tilt and strain deformation induced by hydrologically active natural fractures: application to the tiltmeters installed in Sainte-Croix-aux-Mines observatory (France). *Geophysical Journal International*, 178, 667–677. https://doi.org/10.1111/j.1365-246X.2009.04197.x

Lowry, A.R. (2006). Resonant slow fault slip in subduction zones forced by climatic load stress. *Nature*, 442, 802–805. https://doi.org/10.1038/nature05055

MacQueen, J. (1967). Some methods for classification and analysis of multivariate observations. *Proceedings of the fifth Berkeley symposium on mathematical statistics and probability,* 1, 281–297. University of California Press, Berkeley, Calif., 1967. https://projecteuclid.org/euclid.bsmsp/1200512992

Milanovic, P.T. (2005). Water resources engineering in karst. *Choice Reviews Online*, 42(5), 42-2822. https://doi.org/10.5860/choice.42-2822

Ogata, Y. (1998). Space-Time Point-Process Models for Earthquake Occurrences. *Annals of the Institute of Statistical Mathematics*, 50, 379–402. https://doi.org/10.1023/A:1003403601725

Oestreicher, N. (2018). Geodetic, hydrologic and seismological signals associated with precipitation and infiltration in the central Southern Alps, New Zealand (Ph.D. Thesis). https://hdl.handle.net/10063/7024

Priolo, E., Romanelli, M., Plasencia Linares, M.P., Garbin, M., Peruzza, L., Romano, M.A., Marotta, P., Bernardi, P., Moratto, L., Zuliani, D., & Fabris, P. (2015). Seismic monitoring of an underground natural gas storage facility: the Collalto seismic network. *Seismological Research Letters,* 86, 109–123. https://doi.org/10.1785/0220140087

Pushpalatha, R., Perrin, C., Le Moine, N., Mathevet, T., & Andréassian, V. (2011). A downward structural sensitivity analysis of hydrological models to improve low-flow simulation. *Journal of hydrology*, 411, 66–76. https://doi.org/10.1016/j.jhydrol.2011.09.034

Rodell, M. (2016). GLDAS Noah Land Surface Model L4 monthly 0.25 x 0.25 degree, Version 2.1. *NASA Goddard Earth Sciences Data and Information Services Center*. https://doi.org/10.5067/sxavczfaqlno

Romano, M.A., Peruzza, L., Garbin, M., Priolo, E., & Picotti, V. (2019). Microseismic Portrait of the Montello Thrust (Southeastern Alps, Italy) from a Dense High Quality Seismic Network. *Seismological Research Letters.* https://doi.org/10.1785/0220180387

Rovida, A., Locati, M., Camassi, R., Lolli, B., & Gasperini, P. (2020). The Italian earthquake catalogue CPTI15. *Bulletin of Earthquake Engineering.* 18(7), 2953-2984. https://doi.org/10.1007/s10518-020-00818-y

Rousseeuw, P.J. (1987). Silhouettes: A graphical aid to the interpretation and validation of cluster analysis. *Journal of Computational and Applied Mathematics* 20, 53–65. https://doi.org/10.1016/0377-0427(87)90125-7

Serpelloni, E., Pintori, F., Gualandi, A., Scoccimarro, E., Cavaliere, A., Anderlini, L., Belardinelli, M.E., & Todesco, M. (2018). Hydrologically Induced Karst Deformation: Insights From GPS Measurements in the Adria-Eurasia Plate Boundary Zone. *Journal of Geophysical Research: Solid Earth,* 123, 4413–4430. https://doi.org/10.1002/2017JB015252

Serpelloni, E., Vannucci, G., Anderlini, L., & Bennett, R.A. (2016). Kinematics, seismotectonics and seismic potential of the eastern sector of the European Alps from GPS and seismic deformation data. *Tectonophysics,* 688, 157–181. https://doi.org/10.1016/j.tecto.2016.09.026

Silverii, F., D'Agostino, N., Métois, M., Fiorillo, F., & Ventafridda, G. (2016). Transient deformation of karst aquifers due to seasonal and multiyear groundwater variations observed by GPS in southern Apennines (Italy). *Journal of Geophysical Research: Solid Earth,* 121, 8315–8337. https://doi.org/10.1002/2016JB013361

Torabi, A., Ellingsen, T.S.S., Johannessen, M.U., Alaei, B., Rotevatn, A., & Chiarella, D. (2019). Fault zone architecture and its scaling laws: where does the damage zone start and stop? *Geological Society, London, Special Publications,* SP496-2018–151. https://doi.org/10.1144/SP496-2018-151

van Dam, T., Wahr, J., Milly, P.C.D., Shmakin, A.B., Blewitt, G., Lavallée, D., & Larson, K.M. (2001). Crustal displacements due to continental water loading. *Geophysical Research Letters*, 28, 651–654. https://doi.org/10.1029/2000GL012120

Watkins, M. M., Wiese, D. N., Yuan, D.-N., Boening, C., & Landerer, F. W. (2015). Improved methods for observing Earth's time variable mass distribution with GRACE. *Journal of Geophysical Research: Solid Earth.* https://doi.org/10.1002/2014JB011547.

Zhuang, J., Ogata, Y., & Vere-Jones, D. (2002). Stochastic Declustering of Space-Time Earthquake Occurrences. *Journal of the American Statistical Association 97(458),* 369–380. https://doi.org/10.1198/016214502760046925